Supplementary Material for Nematic Pairing from Orbital Selective Spin Fluctuations in FeSe

Lara Benfatto,[1] Belén Valenzuela,[2] and Laura Fanfarillo[3,*]

[1] *ISC-CNR and Department of Physics, "Sapienza" University of Rome, P.le A. Moro 5, 00185, Rome, Italy*
[2] *Materials Science Factory, Instituto de Ciencia de Materiales de Madrid, ICMM-CSIC, Cantoblanco, E-28049 Madrid, Spain*
[3] *CNR-IOM and International School for Advanced Studies (SISSA), Via Bonomea 265, I-34136, Trieste, Italy*

(Dated: October 11, 2018)

Supplementary Note 1: Band structure

To describe the band structure of FeSe above the superconducting (SC) transition, we adapt the orbital model of ref. 1. The effective band-mass parameters are extracted from ARPES measurements. These values, considerably smaller than the ones predicted by LDA, are usually reproduced remarkably well by DMFT-based calculations[2]. However, both LDA and DMFT fail in the description of the measured Fermi surface (FS), that are always smaller than expected. Such a FS shrinking[3], present already well above the nematic transition[4,5], and the nematic splitting, can be explained instead within our low-energy approach by accounting for the orbital selective spin fluctuations (OSSF). As detailed in ref. 4, the orbital-dependent self-energy corrections due to the exchange of spin fluctuations at $\mathbf{Q}_X$ and $\mathbf{Q}_Y$ lead in general to a temperature-dependent FS shrinking. Due to the anisotropy of the OSSF in a spin-nematic transition, this results in the nematic orbital splitting below T_s.

To illustrate the model, let us start from the low-energy Hamiltonian around the Γ point in the orbital space:

$$H^{\Gamma} = \sum_{\mathbf{k},\sigma} \psi^{\Gamma,\dagger}_{\mathbf{k}\sigma} \hat{H}^{\Gamma}_{0\mathbf{k}} \psi^{\Gamma}_{\mathbf{k}\sigma}. \tag{S1}$$

Here the spinor is defined as $\psi^{\Gamma}_{\mathbf{k},\sigma} = (c_{yz,\mathbf{k},\sigma}, c_{xz,\mathbf{k},\sigma})$. Taking into account the real part of the isotropic Σ^{Γ}_0 and anisotropic $\Delta\Sigma_h$ components of the self-energy, responsible for the nematic shrinking, one has that:

$$\hat{H}^{\Gamma} = \begin{pmatrix} h^{\Gamma}_{0\mathbf{k}} + \Sigma^{\Gamma}_0 + h^{\Gamma}_{3\mathbf{k}} - \Delta\Sigma_h & h^{\Gamma}_{1\mathbf{k}} \\ h^{\Gamma}_{1\mathbf{k}} & h^{\Gamma}_{0\mathbf{k}} + \Sigma^{\Gamma}_0 - h^{l}_{3\mathbf{k}} + \Delta\Sigma_h \end{pmatrix} \tag{S2}$$

where the $h^{\Gamma}_{i,\mathbf{k}}$ components read

$$\begin{aligned} h^{\Gamma}_{0,\mathbf{k}} &= \epsilon_{\Gamma} - a_{\Gamma}\mathbf{k}^2, \\ h^{\Gamma}_{1,\mathbf{k}} &= -2b_{\Gamma}k_x k_y, \\ h^{\Gamma}_{3,\mathbf{k}} &= b_{\Gamma}(k_x^2 - k_y^2), \end{aligned} \tag{S3}$$

and we defined $\Sigma^{\Gamma}_0 \equiv (\Sigma^{\Gamma}_{xz} + \Sigma^{\Gamma}_{yz})/2$ and $\Delta\Sigma_h \equiv (\Sigma^{\Gamma}_{xz} - \Sigma^{\Gamma}_{yz})/2$. As discussed in ref.s 3,4 the self-energy corrections are negative at the hole pocket, so the Σ^{Γ}_0 term accounts in general for an uniform shrinking of the pocket, present already in the paramagnetic phase. Below the structural transition temperature, T_S, nematic spin fluctuations induce larger corrections in the $\mathbf{Q}_X$ direction, which translate in a $|\Sigma^{\Gamma}_{yz}| > |\Sigma^{\Gamma}_{xz}|$, so that $\Delta\Sigma_h > 0$ (ref.4). Taking into account also the spin-orbit splitting it is easy to see[1] that the Hamiltonian (S2) gets an additional term $\pm\lambda/2\hat{\sigma}_2$ in the $\pm$ spin sector. As a consequence the eigenvalues defining the bands are given by:

$$\varepsilon_{\Gamma,\mathbf{k},\pm} = h^{\Gamma}_{0,\mathbf{k}} - |\Sigma^{\Gamma}_0| \pm \sqrt{{h^{\Gamma}_{1,\mathbf{k}}}^2 + (h^{\Gamma}_{3,\mathbf{k}} - \Delta\Sigma_h)^2 + (\lambda/2)^2}, \tag{S4}$$

where the $+/-$ refers to the outer/inner pocket, respectively. Since the two spin sectors have the same energy dispersion we drop from now on any explicit dependence on the spin index. By introducing the orbital weights:

$$\begin{aligned} u^2_{\Gamma,\mathbf{k}} &= \frac{1}{2}\left(1 + \frac{h^{\Gamma}_{3,\mathbf{k}} - \Delta\Sigma_h}{\sqrt{{h^{\Gamma}_{1,\mathbf{k}}}^2 + (h^{\Gamma}_{3,\mathbf{k}} - \Delta\Sigma_h)^2 + (\lambda/2)^2}}\right) \\ v^2_{\Gamma,\mathbf{k}} &= \frac{1}{2}\left(1 - \frac{h^{\Gamma}_{3,\mathbf{k}} - \Delta\Sigma_h}{\sqrt{{h^{\Gamma}_{1,\mathbf{k}}}^2 + (h^{\Gamma}_{3,\mathbf{k}} - \Delta\Sigma_h)^2 + (\lambda/2)^2}}\right) \end{aligned} \tag{S5}$$

one can also define the rotation from the orbital to the band basis

$$\begin{pmatrix} h_{+,\mathbf{k}} \\ h_{-,\mathbf{k}} \end{pmatrix} = \begin{pmatrix} u_{\Gamma,\mathbf{k}} & -v_{\Gamma,\mathbf{k}} \\ v_{\Gamma,\mathbf{k}} & u_{\Gamma,\mathbf{k}} \end{pmatrix} \begin{pmatrix} c_{yz,\mathbf{k}} \\ c_{xz,\mathbf{k}} \end{pmatrix} \tag{S6}$$

where $h^{\dagger}_{+}/h^{\dagger}_{-}$ is the creation operator of a quasiparticle in the outer/inner pocket, respectively. Since in FeSe only the outer pocket crosses the Fermi level, throughout the main text we dropped the + index and we simply referred to $h_{\mathbf{k}}$ and $\varepsilon_{\Gamma,\mathbf{k}}$ as the fermionic operator and bare dispersion of the outer hole pocket. In the paramagnetic phase ($\Delta\Sigma_h = 0$) and in the absence of spin-orbit interaction the two hole bands have a simple parabolic dispersion $\varepsilon_{\Gamma,\mathbf{k},\pm} = \varepsilon_{\Gamma} - |\Sigma^{\Gamma}_0| - (a_{\Gamma} \mp b_{\Gamma})\mathbf{k}^2$. In this case the orbital weights only depend on the azimuthal angle θ measured with respect to $k_x = 0$, so that $u_{\Gamma,\mathbf{k}} = \cos\theta$ and $v_{\Gamma,\mathbf{k}} = \sin\theta$. However, the spin-orbit interaction and the nematic splitting mix the two orbital characters, leading to the angular dependence of the orbital weights at the Fermi level shown in Fig. 2d of the main text.

For the X/Y pockets the general structure is analogous to Eq. (S1), provided that the spinors are now defined as $\psi^{X}_{\mathbf{k}} = (c_{yz,\mathbf{k}}, c_{xy,bk})$ and $\psi^{Y}_{\mathbf{k}} = (c_{xz,\mathbf{k}}, c_{xy,\mathbf{k}})$. In addition,

since the xy orbital is not affected by OSSF, one has in general

$$\hat{H}^X_{\mathbf{k}} = \begin{pmatrix} h^X_{0,\mathbf{k}} + \Sigma^X + h^X_{3,\mathbf{k}} & -ih^X_{2,\mathbf{k}} \\ ih^X_{2,\mathbf{k}} & h^X_{0,\mathbf{k}} - h^X_{3,\mathbf{k}} \end{pmatrix} \quad \text{(S7)}$$

for the X pocket, with

$$\begin{aligned} h^X_{0,\mathbf{k}} &= (h_{yz,\mathbf{k}} + h_{xy,\mathbf{k}})/2 \\ h^X_{2,\mathbf{k}} &= vk_y \\ h^X_{3,\mathbf{k}} &= (h_{yz,\mathbf{k}} - h_{xy,\mathbf{k}})/2 - b(k_x^2 - k_y^2) \end{aligned} \quad \text{(S8)}$$

where $h_{yz,\mathbf{k}} = -\epsilon_{yz} + a_{yz}\mathbf{k}^2$ and $h_{xy,\mathbf{k}} = -\epsilon_{xy} + a_{xy}\mathbf{k}^2$. Analogous expressions hold for the Y pocket provided that one exchange the role of k_x and k_y, $h^Y_{i_\mathbf{k}}(k_x, k_y) = h^X_{i,\mathbf{k}}(k_y, k_x)$, and Σ^X_{yz} is replaced by Σ^Y_{xz}. At the electron pockets the self-energy corrections are positive, so that the $\Sigma^{X/Y}_{yz/xz}$ terms lead again to an upward shift of the yz/xz orbitals. In the spin-nematic state $\Sigma^X_{yz} > \Sigma^Y_{xz}$ so the yz sector of the X pocket shrinks further and the xz part of the Y pocket expands, see Fig. 1 in the main text. The nematic order parameter at the electron pockets is then defined as $\Delta\Sigma_e = (\Sigma^X_{yz} - \Sigma^Y_{xz})/2 > 0$. Notice that in our approach the change of sign of the nematic splitting at the Γ and $M = (X, Y)$ point is a natural consequence of the self-energy corrections induced by nematic OSSF, as explained in[4]. The X/Y band dispersions are given by

$$\varepsilon^{X/Y}_{\mathbf{k},\pm} = h^{X/Y}_{0,\mathbf{k}} + \Sigma^X/2 \pm \sqrt{{h^X_{2,\mathbf{k}}}^2 + (h^X_{3,\mathbf{k}} - \Sigma^X_{yz}/2)^2}, \quad \text{(S9)}$$

such that $\varepsilon^{X/Y}_{\mathbf{k},+}$ is the electronic band crossing the Fermi level at the X/Y point. The rotation from the orbital to the band basis is defined now as

$$\begin{pmatrix} e_{X,\mathbf{k},+} \\ e_{X,\mathbf{k},-} \end{pmatrix} = \begin{pmatrix} u_{X,\mathbf{k}} & -iv_{X,\mathbf{k}} \\ iv_{X,\mathbf{k}} & u_{X,\mathbf{k}} \end{pmatrix} \begin{pmatrix} c_{yz,\mathbf{k}} \\ c_{xy,\mathbf{k}} \end{pmatrix} \quad \text{(S10)}$$

with the orbital weights given by

$$\begin{aligned} u^2_{X,\mathbf{k}} &= \frac{1}{2}\left(1 + \frac{h^X_{3,\mathbf{k}} - \Sigma^X_{yz}/2}{\sqrt{{h^X_{2,\mathbf{k}}}^2 + (h^X_{3,\mathbf{k}} - \Sigma^X_{yz}/2)^2}}\right), \\ v^2_{X,\mathbf{k}} &= \frac{1}{2}\left(1 - \frac{h^X_{3,\mathbf{k}} - \Sigma^X_{yz}/2}{\sqrt{{h^X_{2,\mathbf{k}}}^2 + (h^X_{3,\mathbf{k}} - \Sigma^X_{yz}/2)^2}}\right), \end{aligned} \quad \text{(S11)}$$

At the Y points the definitions are again equivalent, provided that one replaces Σ^X_{yz} with Σ^Y_{xz} and k_x with k_y. As for the hole pocket, we drop the + index and we refer to $e_{X/Y,\mathbf{k}}$ and $\varepsilon_{X/Y,\mathbf{k}}$ as the fermionic operators and energy dispersions of the electronic X/Y pockets. In summary, the notations used in the main text are:

$$\begin{aligned} \varepsilon_{\Gamma,\mathbf{k},+} &\to \varepsilon_{\Gamma,\mathbf{k}} \quad h_{+,\mathbf{k}} \to h_{\mathbf{k}} \quad \text{hole pocket} \\ \varepsilon_{X,\mathbf{k},+} &\to \varepsilon_{X,\mathbf{k}} \quad e_{X,\mathbf{k},+} \to e_{X,\mathbf{k}} \quad X \text{ pocket} \\ \varepsilon_{Y,\mathbf{k},+} &\to \varepsilon_{Y,\mathbf{k}} \quad e_{Y,\mathbf{k},+} \to e_{Y,\mathbf{k}} \quad Y \text{ pocket} \end{aligned}$$

With these definitions in mind the rotation from the orbital to the band basis defined in Eq.s (1)-(3) of the main text are equivalent to Eq. (S6) and (S10) above.

Finally, we notice that the present low-energy model describes properly the orbital character of the bands up to energy scale of order of 0.5 eV around the Fermi level, beyond which additional d orbitals should be taken into account[6]. Since both the nematic and SC transition involved much smaller energy scales, the results obtained within the present low-energy approach are expected to be robust with respect to the band-structure description obtained within more sophisticated five- or ten-orbital models.

Supplementary Note 2: Orbital Selective Spin Fluctuations Model

Once established the orbital composition of the low-energy model, one can project the general interacting Hamiltonian including the Hubbard and Hund terms into the low-energy states. As shown in[7,8] one obtains that the effective low-energy interacting terms can be written as

$$H_{int} = -\frac{\tilde{U}}{2}\sum_{\mathbf{q}} \mathbf{S}^{yz/xz}_{X/Y} \cdot \mathbf{S}^{yz/xz}_{X/Y}. \quad \text{(S12)}$$

Here $\tilde{U}$ is the intraorbital interaction renormalized at low energy and the intraorbital spin operators connecting hole and electron pocket are given by Eq.s (4)-(5) of the main text, that we rewrite here explicitly including also the contribution of the inner pocket, when present:

$$\begin{aligned} \mathbf{S}^{yz}_X &= \sum_{\mathbf{k}} (u_\Gamma h^\dagger_+ + v_\Gamma h^\dagger_-)\, \vec{\sigma}\, u_X e_X, \quad \text{(S13)} \\ \mathbf{S}^{xz}_Y &= \sum_{\mathbf{k}} (-v_\Gamma h^\dagger_+ + u_\Gamma h^\dagger_-)\, \vec{\sigma}\, u_Y e_Y, \quad \text{(S14)} \end{aligned}$$

where momentum dependence has been dropped for simplicity. The low-energy interacting Hamiltonian in Eq.(S12) defines the OSSF: at low energy the hole pockets at Γ and the X/Y electron pockets share only one orbital, the yz/xz respectively. Thus the spin interactions along x and y has a single orbital character (see Fig 1 in the main text):

$$\begin{aligned} \langle \mathbf{S}\cdot\mathbf{S}\rangle(\mathbf{Q}_X) &\Rightarrow \langle \mathbf{S}^{yz}_X \cdot \mathbf{S}^{yz}_X\rangle \\ \langle \mathbf{S}\cdot\mathbf{S}\rangle(\mathbf{Q}_Y) &\Rightarrow \langle \mathbf{S}^{xz}_Y \cdot \mathbf{S}^{xz}_Y\rangle \end{aligned} \quad \text{(S15)}$$

By computing self-energy corrections of the orbital states coming from these OSSF one obtains orbital-dependent self-energy corrections, as shown in Eq. (S2) and (S7) above. In addition, within a spin-nematic scenario the anisotropy of the spin fluctuations at different $\mathbf{Q}$ vectors translates in the nematic splitting $\Delta\Sigma_h$, $\Delta\Sigma_e$ of the orbitals discussed previously. Here we argue that OSSF can also mediate an orbital-selective nematic pairing. The

pairing model mediated by OSSF can be easily derived by rewriting the spin-spin interaction terms (S12) in the pairing channel, using the projection of the orbital spin operator on the band basis encoded in Eq.s (S13)-(S14) above. The resulting pairing interaction is given by Eq. (8) of the main text.

Supplementary Note 3: Model parameters for FeSe

We solve self-consistently the set of BCS equations for realistic parameters for the FeSe system in the nematic phase.

Although the physical outcome of this work does not crucially depend on this, instead of using exactly the band parameters of ref. 4, we will adjust them to fit a smaller value of the nematic splitting of the electron pockets reported afterwards in the literature, $\Delta\Sigma_e \simeq 15$ meV[9–11]. When computing self-consistently the spectral function of electrons coupled to spin modes in ref. 4, we included the full frequency-dependent self-energies, thus we also effectively included the quasiparticle weight Z_{spin} due to the orbital-dependent mass renormalization. However, since we checked that Z_{spin} was of order one for the various orbitals, to reduce the number of parameters we decided in the present work to choose directly the band parameters which reproduce the experimental dispersions. This explains the small quantitative differences between the values listed in Table S1 and those listed in ref. 4. The list of the band parameters appearing in Eq.s (S3), (S8) and used in the calculations are given in Table S1. The spin-orbit coupling is assumed λ= 20 meV. We use $|\Sigma^{\Gamma}_{yz/xz}| = 70/40$ meV and $\Sigma^{X/Y}_{yz/xz} = 45/15$ meV, in order to have $\Delta\Sigma_{h/e} = 15$ meV.

Γ		X			
ϵ_Γ	46	ϵ_{xy}	72	ϵ_{yz}	55
a_Γ	263	a_{xy}	93	a_{yz}	101
b_Γ	182	b	154		
		v	144		

TABLE S1: Low-energy model parameters for FeSe in the nematic phase at $k_z = 0$. All the parameters are in meV, the k vector is measured in units $1/a \sim 0.375$ Å, where $a = a_{FeFe}$ is the lattice constant of the 1-Fe unit cell (so that $\tilde{a} = \sqrt{2}a = 3.77$ Å is the lattice constant of the 2Fe unit cell).

The u, v, factors defined by Eq.s (S5), (S11), computed using the above set of parameters, are shown in Fig. 2 of the main text. We reproduce the FS and their orbital distribution as experimentally observed by ARPES at $k_z = 0$ (ref.s 4,9–12), with the hole pocket having $k^x_F = 0.056$ Å^{-1} and $k^y_F = 0.11$ Å^{-1}, the X one $k^x_F = 0.20$ Å^{-1} and $k^y_F = 0.051$ and the Y, $k^x_F = 0.10$ and $k^y_F = 0.20$ Å^{-1} in the nematic phase.

Using now the $T = 0$ BCS equations, Eq.s (10)-(15) of the main text, we can fit the experimental data of ref. 13 using the SC couplings as fitting parameters. The results for the orbital SC order parameters, Eq.s (10)-(15), are listed in Table S2 while in Fig. 4 of the main text we showed the band gaps, Eq.s (16)-(18) of the main text. Notice that assuming isotropic pairing interactions $g_X = g_Y = 1.03$ eV and accounting only for the orbital splitting effects, encoded in the u, v factors, the SC gap at Γ presents opposite anisotropy with respect the one found in the experiment. On the other hand, considering nematic pairing, $g_X/g_Y = 21$, with g_X=5.88 eV> g_Y = 0.28 eV we reproduce both the absolute values and the angular modulation of the observed gap at Γ and X. For sake of completeness in Fig.4 we show the results obtained including the xy-pairing channel. We use $g_{xy} = -0.45$ eV in order to reproduce the experimental data from ref. 13. The inclusion of such contribution does not affect the discussion above. Notice that our results are rather robust with respect to small variations of the band parameters and nematic splitting. For example, a larger nematic splitting $\Delta\Sigma_e = 20$ at M as initially estimated in ref. 4, would not alter our results, see Fig. S1. The only difference is that in this case one has a larger gain from the orbital ordering at M, so that the experimental data are reproduced with a slightly smaller nematic pairing $g_X/g_Y = 19$.

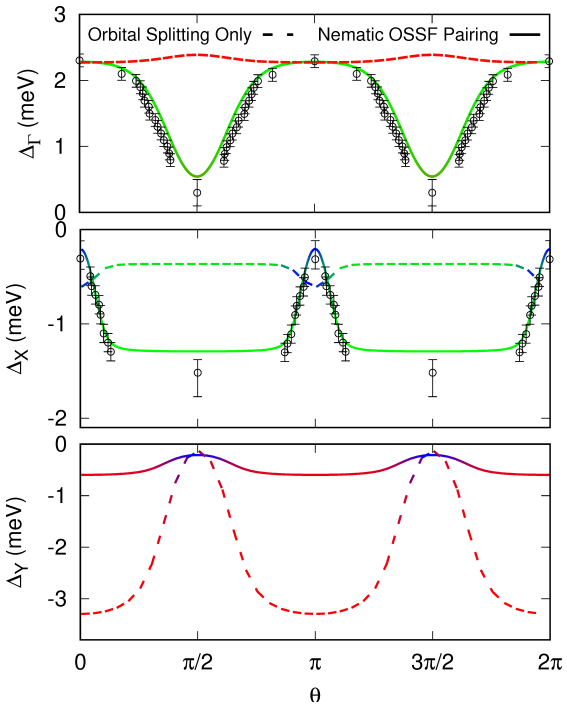

FIG. S1: Numerical results for the band gaps on the Γ (top), X (middle) and Y (bottom) pocket obtained considering a larger nematic splitting at M, $\Delta\Sigma_e = 20$ meV.

It is interesting to compare the value of the anisotropy obtained here with the anisotropy of the OSSF extracted from the analysis of the shrinking effect in ref. 4. In ref. 4 the spectral function of the spin modes along the two

Δ_h^{yz}	Δ_h^{xz}	Δ_e^{yz}	Δ_e^{yz}	Δ_X^{xy}	Δ_Y^{xy}
15.71	0.19	−1.46	−0.71	−0.20	−0.23

TABLE S2: $T = 0$ orbital SC order parameters (in meV) of the band gap shown in Fig 4 of the main text.

directions has been modelled as:

$$B_{X/Y}(\omega) = \frac{1}{\pi}\frac{\omega\omega_0}{\omega_{X/Y}^2 + \omega^2}. \tag{S16}$$

While at RPA level the spin modes are always degenerate, taking into account spin-spin interactions beyond Gaussian level[8,14] one can show that below T_S spin fluctuations break the Z_2 Ising degeneracy and they become stronger at a given $\mathbf{Q}$ vector. This is encoded in Eq. (S16) above with two anisotropic masses $\omega_{X/Y}$ below T_S. The analysis of the orbital ordering induced by OSSF discussed in[4] and outlined above shows that below T_S one should then have stronger spin fluctuations at $\mathbf{Q}_X$, which implies $\omega_X < \omega_Y$ and $V_X > V_Y$, where $V_{X/Y}$ is the coupling of the fermions to the spin modes. The strength of the pairing interaction is given by the product of the real part $\chi'_{X/Y}(\omega = 0)$ of the spin-fluctuation propagator at $\omega = 0$ times the spin-mode coupling $V_{X/Y}$. Using then the Kramers-Kronig relation of χ' to the spectral function (S16) we get:

$$\begin{aligned} g_{X/Y} \;&\propto\; V_{X/Y}\chi'_{X/Y}(\omega = 0) = V_{X/Y}\int d\omega \frac{B_{X/Y}(\omega)}{\omega} = \\ &=\; V_{X/Y}\frac{\omega_0}{\omega_{X/Y}} \end{aligned} \tag{S17}$$

The analysis of ARPES measurements performed in ref. 4 gives at $T > T_c$ $\omega_Y/\omega_X = 1.6$ and $V_X/V_Y = 8$. Here we used, in the notation of ref. 4, the values of the coupling $V^{eh}_{X/Y}$. With these numbers we obtain $g_X/g_Y = 13.4$, a ratio of the same order of magnitude of what we extracted from the gap anisotropy $g_X/g_Y = 21$. Notice that the present estimate does not take into account the feedback of the SC order on the spin modes and could explain the difference between the two results. Such a full self-consistent treatment is beyond the scope of the present manuscript and will be addressed in a future work.

Let us finally address the issue of the k_z gap dependence. As discussed in the main text, a crucial difference when moving from $k_z = 0$ to $k_z = \pi$ is that the orbital character of the hole pocket changes considerably. Since all the FS pockets expand[15–17], the effect of the nematic order is less dramatic on the hole pocket, with the consequence that it retains full yz character at $\theta = 0$[16]. This has already a profound impact on the hole-gap anisotropy, as recently pointed out in ref. 18. To highlight the effect of the change of orbital weights on the hole pocket at Z we analyze the BCS solution using a set of realistic band parameters for the Z-pocket as listed in Table S3.

Z	
ϵ_Z	26
a_Z	473
b_Z	264

TABLE S3: Low-energy model parameters for the hole-pocket at $k_z = \pi$ in the nematic phase.

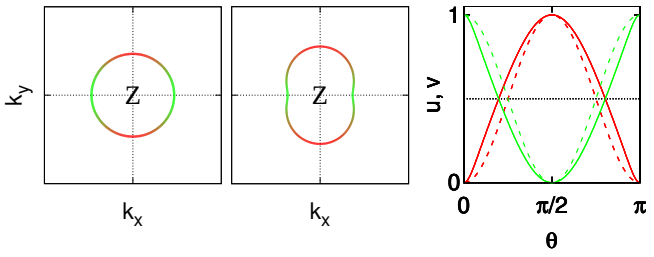

FIG. S2: $k_z = \pi$ cut of the FS FeSe in the (a) paramagnetic and (b) nematic phase. The colors represent the main orbital character. (c) Orbital component amplitude of the FS as a function of the azimuthal angle theta in the tetragonal (dashed lines) and nematic phase (solid lines)

In the absence of a detailed comparison with the band structure above T_S as done in ref. 4, we already include in ϵ_Z the effect of the isotropic shrinking, $(\Sigma^\Gamma_{yz}+\Sigma^\Gamma_{xz})/2$, and consider separately a further nematic splitting $\Delta\Sigma_h = 10$ meV. In Fig. S2 we show the FS shape and composition of the Z pocket in both the paramegnetic and nematic phase. Notice that even below T_s, the large elliptical Z pocket, $k^x_F = 0.10$ Å^{-1} and $k^y_F = 0.15$ Å^{-1}, retains a marked yz character at $\theta = 0$ in agreement with the ARPES measurements[15–17]. Moreover given this band structure, the inclusion of a finite spin-orbit coupling does not lead to any significant change, and the u_Z, v_Z, factors defined as Eq.s (S5), (S11) scale approximately as $\cos\theta$ and $\sin\theta$ even below T_s.

Solving the BCS equation in this case one can easily check that, contrary to what found at $k_z = 0$, $\langle u^4_Z\rangle \sim \langle v^4_Z\rangle$, so that the increase of the $\langle u^4_X\rangle$ factor over the $\langle u^4_Y\rangle$ in the nematic phase is enough to have $\Delta^{yz}_h > \Delta^{xz}_h$. In this case already without nematic pairing one has a larger gap value at $\theta = 0$, as observed indeed in ref. 18 (see also Fig 5 in the main text). As a consequence, if one retains instead the pairing anisotropy g_X/g_Y extracted from the fitting of the $k_z = 0$ gaps the anisotropic effect due to the nematic pairing is amplified now by the orbital factors that cooperates to give the same gap modulation. As a result we would get larger gap values and larger anisotropy when moving from the Γ to the Z pocket. Recent ARPES experiments investigated the SC gaps at $k_z = \pi$[12,15–17]. While all the experiments confirm the in-plane anisotropy of the gap of the hole-pocket, with a larger gap value at $\theta = 0$, the various reports are somehow in disagreement on the k_z dependence of the gap-magnitude. In fact in ref.s 15,17

the absolute value of the gap and its anisotropy are found to be larger at $k_z = \pi$, while in ref.s 12,16 the authors claimed a decreasing of the gap magnitude when moving from the Γ to the Z pocket. The present situation calls for a more detailed experimental analysis and specific theoretical studies involving a 3D modeling of the band structure. As a matter of fact, details of the 3D band model could change the estimate of the magnitude of the gaps at different k_z, influencing the orbital ordering effects and the balance between such mechanism and the nematic pairing one. For example, in ref. 18 the authors obtain a larger anisotropy $\Delta_{max}/\Delta_{min}$ at the Z pocket than in our case. This is possibly due to a much larger suppression of xz character at the Y pocket in their model, leading to a larger $\langle u_X^4 \rangle \gg \langle u_Y^4 \rangle$ anisotropy at the electron pockets. Unfortunately, the controversy on the observation of the Y pocket in ARPES[12,17] does not allow us to disentangle this issue experimentally. Finally, notice that the authors of ref. 18 do not solve the self-consistent equations at $T = 0$, as we do, but the linearized ones near T_c. Since in a multiband system the ratios of the gaps in the various bands depend on temperature, one cannot trivially compare those results with the one discussed in the present manuscript. Nonetheless, the main qualitative findings, and in particular the wrong gap anisotropy found at Γ without nematic pairing, hold in both works, apart from possible quantitative differences.

* corresponding author: laura.fanfarillo@sissa.it

[1] Cvetkovic, V. & Vafek, O. Space group symmetry, spin-orbit coupling, and the low-energy effective hamiltonian for iron-based superconductors. Phys. Rev. B **88**, 134510 (2013).

[2] de' Medici, L., Giovannetti, G. & Capone, M. Selective mott physics as a key to iron superconductors. Phys. Rev. Lett. **112**, 177001 (2014).

[3] Ortenzi, L., Cappelluti, E., Benfatto, L. & Pietronero, L. Fermi-surface shrinking and interband coupling in iron-based pnictides. Phys. Rev. Lett. **103**, 046404 (2009).

[4] Fanfarillo, L. et al. Orbital-dependent fermi surface shrinking as a fingerprint of nematicity in fese. Phys. Rev. B **94**, 155138 (2016).

[5] Kushnirenko, Y. S. et al. Anomalous temperature evolution of the electronic structure of fese. Phys. Rev. B **96**, 100504 (2017).

[6] Fernandes, R. M. & Chubukov, A. V. Low-energy microscopic models for iron-based superconductors: a review. Reports on Progress in Physics **80**, 014503 (2017).

[7] Fanfarillo, L., Cortijo, A. & Valenzuela, B. Spin-orbital interplay and topology in the nematic phase of iron pnictides. Phys. Rev. B **91**, 214515 (2015).

[8] Fanfarillo, L., Benfatto, L. & Valenzuela, B. Orbital mismatch boosting nematic instability in iron-based superconductors. Phys. Rev. B **97**, 121109 (2018).

[9] Fedorov, A. et al. Effect of nematic ordering on electronic structure of fese. Scientific reports **6**, 36834 (2016).

[10] Watson, M. D., Haghighirad, A. A., Rhodes, L. C., Hoesch, M. & Kim, T. K. Electronic anisotropies revealed by detwinned angle-resolved photo-emission spectroscopy measurements of fese. New Journal of Physics **19**, 103021 (2017).

[11] Coldea, A. I. & Watson, M. D. The key ingredients of the electronic structure of fese. Annual Review of Condensed Matter Physics **9**, 125–146 (2018).

[12] Rhodes, L. C. et al. Scaling of the superconducting gap with orbital character in fese. arXiv preprint arXiv:1804.01436 (2018).

[13] Sprau, P. O. et al. Discovery of orbital-selective cooper pairing in fese. Science **357**, 75–80 (2017).

[14] Fernandes, R. M., Chubukov, A. V., Knolle, J., Eremin, I. & Schmalian, J. Preemptive nematic order, pseudogap, and orbital order in the iron pnictides. Phys. Rev. B **85**, 024534 (2012).

[15] Xu, H. C. et al. Highly anisotropic and twofold symmetric superconducting gap in nematically ordered $fese_{0.93}s_{0.07}$. Phys. Rev. Lett. **117**, 157003 (2016).

[16] Hashimoto, T. et al. Superconducting gap anisotropy sensitive to nematic domains in fese. Nature communications **9**, 282 (2018).

[17] Kushnirenko, Y. S. et al. Three-dimensional superconducting gap in fese from angle-resolved photoemission spectroscopy. Phys. Rev. B **97**, 180501 (2018).

[18] Kang, J., Fernandes, R. M. & Chubukov, A. Superconductivity in fese: The role of nematic order. Phys. Rev. Lett. **120**, 267001 (2018).